Spectrochimica Acta Part A: Molecular and Biomolecular Spectroscopy 251 (2021) 119422

Contents lists available at ScienceDirect

Spectrochimica Acta Part A: Molecular and Biomolecular Spectroscopy

journal homepage: www.elsevier.com/locate/saa

Mid-infrared spectroscopy as process analytical technology tool for estimation of THC and CBD content in Cannabis flowers and extracts

Nikola Geskovski [a,*], Gjose Stefkov [b], Olga Gigopulu [c], Stefan Stefov [d], Christian W. Huck [e], Petre Makreski [f,*]

[a] Institute of Pharmaceutical Technology, Faculty of Pharmacy, Ss Cyril and Methodius University, Majka Tereza 47, 1000 Skopje, North Macedonia
[b] Institute of Pharmacognosy, Faculty of Pharmacy, Ss Cyril and Methodius University, Majka Tereza 47, 1000 Skopje, North Macedonia
[c] Institute of Applied Chemistry and Pharmaceutical Analysis, Faculty of Pharmacy, Ss Cyril and Methodius University, Majka Tereza 47, 1000 Skopje, North Macedonia
[d] ReplekFarm, Kozle 188, Skopje, North Macedonia
[e] Institute of Analytical Chemistry and Radiochemistry, CCB – Center for Chemistry and Biomedicine, Leopold-Franzens University, Innrain 80-82, 6020 Innsbruck, Austria
[f] Institute of Chemistry, Faculty of Natural Sciences and Mathematics, Ss Cyril and Methodius University, Arhimedova 5, 1000 Skopje, North Macedonia

HIGHLIGHTS

- Mid-IR spectra revealed distinctive features and bands between THC(A) and CBD(A).
- FTIR quantification of THC and CBD in Cannabis flowers and extracts was performed.
- PLS models using 2nd derivative of 1800–400 cm^{-1} spectral region were constructed.
- Statistical output points to favorable THC and CBD content prediction capabilities.

GRAPHICAL ABSTRACT

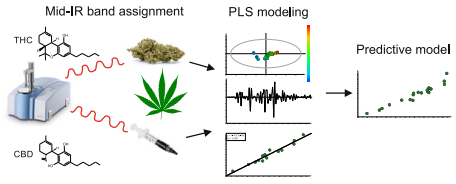

ARTICLE INFO

Article history:
Received 6 November 2020
Received in revised form 24 December 2020
Accepted 30 December 2020
Available online 05 January 2021

Keywords:
Tetrahydrocannabinol (THC)
cannabidiol (CBD)
Mid-infrared spectroscopy
Cannabis flower
Cannabis extract
Partial least-squares (PLS)

ABSTRACT

Tetrahydrocannabinol (THC) and cannabidiol (CBD) are the most notable Cannabis components with pharmacological activity and their content in the plant flowers and extracts are considered as critical quality parameters. The new Medical Cannabis industry needs to adopt the quality standards of the pharmaceutical industry, however, the variability of phytocannabinoids content in the plant material often exerts an issue in the inconsistency of the finished product quality parameters. Sampling problems and sample representativeness is a major limitation in the end-point testing, particularly when the expected variation of the product quality parameters is high. Therefore, there is an obvious need for the introduction of Process Analytical Technology (PAT) for continuous monitoring of the critical quality parameters throughout the production processes. Infrared spectroscopy is a promising analytical technique that is consistent with the PAT requirements and its implementation depends on the advances in instrumentation and chemometrics that will facilitate the qualitative and quantitative aspects of the technique. Our present work aims in highlighting the potential of mid-infrared (MIR) spectroscopy as PAT in the quantification of the main phytocannabinoids (THC and CBD), considered as critical quality/-material parameters in the production of Cannabis plant and extract. A detailed assignment of the bands related to the molecules of interest (THC, CBD) was performed, the spectral features of the decarboxylation of native flowers were identified, and the specified bands for the acid forms (THCA, CBDA) were assigned and thoroughly explained. Further, multivariate models were constructed for the prediction of both THC and CBD content in extract and flower samples from various origins, and their prediction ability was tested on a separate sample set. Savitskzy-Golay smoothing and the second derivative of the native MIR spectra (1800–400 cm^{-1} region) resulted in best-fit parameters. The PLS models presented

* Corresponding authors.
E-mail addresses: ngeskovski@ff.ukim.edu.mk (N. Geskovski), petremak@pmf.ukim.mk (P. Makreski).

https://doi.org/10.1016/j.saa.2020.119422

satisfactory R2Y and RMSEP of 0.95 and 3.79% for THC, 0.99 and 1.44% for CBD in the Cannabis extract samples, respectively. Similar statistical indicators were noted for the Partial least-squares (PLS) models for THC and CBD prediction of decarboxylated Cannabis flowers (R2Y and RMSEP were 0.99 and 2.32% for THC, 0.99 and 1.33% for CBD respectively). The VIP plots of all models demonstrated that the THC and CBD distinctive band regions bared the highest importance for predicting the content of the molecules of interest in the respected PLS models. The complexity of the sample (plant tissue or plant extract), the variability of the samples regarding their origin and horticultural maturity, as well as the non-uniformity of the plant material and the flower-ATR crystal contact (in the case of Cannabis flowers) were governing the accuracy descriptors. Taking into account the presented results, ATR-MIR should be considered as a promising PAT tool for THC and CBD content estimation, in terms of critical material and quality parameters for Cannabis flowers and extracts.

1. Introduction

Cannabis sativa L., Cannabaceae, has a long history of exploitation as a medicine, in pain relief and epilepsy, and also in food, textile, and paper industries [1,2]. The scientific research of *Cannabis sativa* demonstrates an exponential increase in the past 30 years, as most of its ingredients were isolated and characterized, but the breakthrough was achieved in the discovery of the endogenous cannabinoids and the endocannabinoid system [3]. Also, many study results, personal and anecdotal testimonies changed the public perception, asserting pressure for legislation changes in the definition of Cannabis as a Schedule 1 substance resulting in passing laws that legalize its use for medical purposes. Even though each country/state that passed such law brought specific provisions that vary considerably (for distribution through dispensaries, permitted amounts per patient), the common feature of these laws is that they permit the legal use of cannabis for medical treatment if the patient has obtained appropriate medical authorization [4].

Such legislation changes paved the road for industrialization of the Cannabis products for medical purposes. However, the new Medical Cannabis industry needs to adopt the quality standards of the pharmaceutical industry and at the same time satisfy the specific requirements of Cannabis-legislation. This means that the Cannabis products for medicinal use need to comply with its established quality parameters and standards and to be manufactured under cGMP regulations.

Tetrahydrocannabinol (THC) and cannabidiol (CBD) are well-known phytocannabinoids, considered as the most notable Cannabis components with pharmacological activity [5]. THC acts mostly as a CB1 receptor agonist, leading to its distinguished psychoactive and pain relief effects, while CBD works through a variety of pharmacological pathways, including inhibition of endocannabinoid reuptake, activation of transient receptor potential vanilloid 1 and G protein-coupled receptor 55 [6,7]. Considering their immense importance in the overall pharmacological activity, as well as the current Cannabis legislation restrictions, related to the THC content of some classes of Cannabis products, one could entitle the content of CBD and THC as critical quality parameters of Cannabis products. The CBD and THC content could also be considered as critical material parameters when Cannabis flowers are used as starting material in the production. The quality control of Cannabis inflorescence and chemotype differentiation is a subject of many Pharmacopoeias [8–11] focus on the assay of the content of five main cannabinoids CBDA, CBD, CBN, Δ^9THC and Δ^9-THCA. The above-referenced Pharmacopoeias comprise monographs on cannabis defining the dried drug or herbal substance "Cannabis inflorescence" that contains a minimum of 90 and a maximum of 110% the amounts of cannabinoids such as Δ^9-THC and CBD, as well as Cannabinoid carboxylic acids such as Δ^9-THCA and CBDA, calculated as Δ^9-THC or CBD, based on the dried drug. Depending on the content of Δ^9-THC and CBD, authorities have classified generally three chemotypes of *Cannabis sativa L.*: Δ^9-THC-predominant type, i.e. drug-type (CBD/Δ^9-THC = 0–0.005), CBD-predominant type, i.e. fiber type ("hemp" type) (CBD/Δ^9-THC = 1 5.0–25.0) and intermediate chemotype (CBD/Δ^9-THC = 0.5–3.0) [12]. Regarding cannabis extracts, so far the German pharmacopeia [8] recognizes discontinued cannabis extract - *Cannabis* extractum normatum defining as an extract from whole or shredded, flowering, dried shoot tips of the female plants of *Cannabis sativa* L. that contains Δ^9-THC at least 1% and at most 25% (m/m) for the extract, and CBD maximum 10% (m/m) for the extract. The chemical complexity of cannabis makes its pharmaceutical standardization challenging. Thus, chemical characterization must include well-defined methodologies that would characterize the plant chemotype and the herbal drug as well as extraction procedures. It was found that the concentrations of target cannabinoids obtained for the same plant chemotype originating from different suppliers could vary for more than 25% [12]. Scientific and technological development in regard to *Cannabis sativa* began, highlighting the need of sensitive, specific and robust analytical methods for identification and quantification of the active constituents of *Cannabis sativa*.

Gas chromatography (GC) and liquid chromatography (HPLC) are regarded as analytical methods of choice for the quantification of phytocannabinoids [13]. Both are relatively slow and costly techniques and require sample preparation that involves at least extraction of the ingredients with organic solvents. Since quality assessment in the current Medical Cannabis industry relies on end-product testing, these techniques are vastly employed. However, the variability of phytocannabinoids content in the plant material often exerts an issue in the inconsistency of the finished product quality parameters. Sampling problems and sample representativeness is a major limitation in the end-point testing, particularly when the expected variation of the product quality parameters is high. Usually, physical limitations (i.e. use of an inappropriate sampling thief, or/and sample volume) prevent the test sample analysis to adequately represent the whole batch variability [14]. Besides, the critical quality parameters are not monitored frequently during the production process, thus lacking the knowledge for appropriate identification of critical process parameters in the process optimization. Therefore, there is an obvious need for the introduction of the concept of quality by design (QbD) in Cannabis products manufacturing, which means that product quality should be scientifically designed to meet specific objectives, not merely empirically derived from the performance of test batches. In this manner, the product and process characteristics important to desired performance must be derived from a combination of prior knowledge and vast experimental assessment during product development. The generated data will result in the construction of a multivariate model linking product and process measurements and desired parameters [15].

Implementation of Process Analytical Technology (PAT) is an important QbD tool aimed to increase the understanding essential for the quality throughout the manufacturing process, which became recognizable in the Pharmaceutical industry by the initiative launched by the FDA [16]. Infrared spectroscopy is a promising analytical technique that is consistent with the PAT requirements of the FDA guidelines, and its implementation depends on the advances in instrumentation and chemometrics that will facilitate the qualitative and quantitative aspects of the technique.

In the literature, few attempts have been made to introduce near-infrared spectroscopy for quantification of phytocannabinoids in plant material [17], in liquid pharma-grade Cannabis formulations [18] and for growth-staging of Cannabis [19]. To the best of our knowledge, so far no scientific papers are addressing the capability of mid-infrared spectroscopy (MIR) for quantification of phytocannabinoids in Cannabis plant material and extract.

Therefore, our present work aims in highlighting the potential of mid-infrared (MIR) spectroscopy as PAT in the quantification of the main phytocannabinoids (THC and CBD), considered as critical quality/material parameters in the production of Cannabis plant and extract. To achieve our goals, we have performed MIR analysis of Cannabis flowers (plant material) and Cannabis extracts from various randomized sources with various CBD and THC content and employed a multivariate statistical approach to develop and optimize the calibration models. Furthermore, a prediction set was used to estimate the prediction capability of each MIR model against the referent analytical technique (HPLC).

Table 1
The content (%) of THC, THCA, CBD, CBDA, total TCH (THCA × 0.877 + THC), and total CBD (CBDA × 0.877 + CBD) in the air-dried non-thermally treated cannabis FL1 and FL2 determined by HPLC.

Cannabinoid	THCA dominant flower (FL1)	CBDA dominant flower (FL2)
CBD	0.03	2.34
CBDA	0.15	20.51
THC	4.19	0.26
THCA	16.23	0.6
Total CBD	0.16	20.33
Total THC	18.42	0.79

2. Materials and methods

2.1. Samples – Thermally untreated air dried Cannabis flowers (FL)

Two *Cannabis sativa* strains, Bedrocan (*Cannabis sativa* L. *'Afina'*) and Bedrolite (*Cannabis sativa* L. *'Elida'*) were obtained. Bedrocan sample features high THCA content and low CBDA content, cultivar type I (FL1), whereas the Bedrolite contains a high content of CBDA and low content of THCA, cultivar type II (FL2). The samples were thermally-unaffected, only left air-dried to obtain maximum 10 wt % water content.

2.2. Samples – Thermally treated Cannabis dry flowers (FLT)

Forty five flowers left for analysis at the Centre for Natural Products Analysis (Faculty of Pharmacy), originating from various and different randomized crops, were used. 0.5 g of each drug was placed in a flask and moved to the oven (120 °C, 60 min) to proceed with the decarboxylation reaction (THCA → THC; CBDA → CBD). Afterward, the samples were immediately subjected to an HPLC analysis to obtain the content of THC and CBD.

2.3. Samples – Cannabis extracts (Ex)

Thirty four Cannabis extracts, supplied from the Centre for Natural Products Analysis (Faculty of Pharmacy), were analyzed. These extracts were randomly prepared and not origin-correlated. The samples were subjected to an HPLC analysis to obtain the content of THC and CBD.

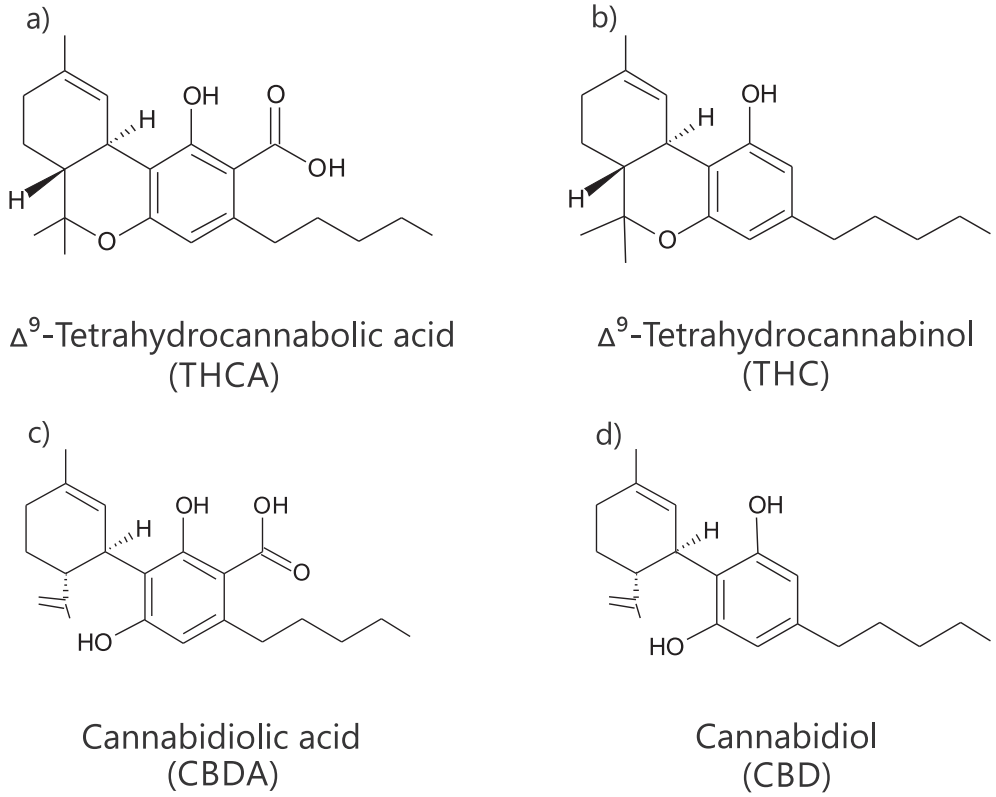

Fig. 1. Structural formulae of the main cannabinoids present in *Cannabis sativa*.

2.4. Standard substances

The CBD powdered standard (>99.5 wt%) originates from GenCanna Global, USA. The THCA analytical powdered standard (98.8 wt%) was supplied from Sigma-Aldrich, USA. Upon decarboxylation to 140 °C, carefully guided and monitored on a hotplate, the THCA standard was quantitatively converted to THC (confirmed by HPLC analysis).

2.5. Mid-infrared spectroscopy

MIR spectra were collected on the attenuated total reflection (ATR) module of an Alpha Platinum ATR Fourier transform infrared spectrometer (Bruker Optik, Germany). Ten milligrams of each dry sample was used for spectral acquisition whereas few drops of each extract were placed on the ATR plate compartment. After the collection of each extract IR spectrum, the solidified specimen that remained on the plate was dissolved in hexane and the compartment was cleaned to proceed with the next extract sample. Each IR spectrum was recorded in the 4000 to 400 cm^{-1} region and averaged from eight scans with the spectral resolution adjusted to 4 cm^{-1}.

2.6. High Performance Liquid Chromatography (HPLC) for the cultivars, FL1 and FL2

The chromatographic analyses for the FL1 and FL2 were performed on an integrated UPLC system Shimadzu Nexera Prominence LC-2030C Plus Cannabis analyzer controlled by Lab Solutions version 5.92. The flow rate was set to 1 mL/min with UV detector monitoring at 220 nm and an injection volume of 5 μL. The mobile phase consisted of 64:36 (*V/V*) acetonitrile and (0.05%) trimethylamine, pH = 3. The HPLC column, Discovery C8 (150x4.6 mm with 5 μm particle size) were purchased from Merck (Darmstadt, Germany). All the chemicals used were of EP grade quality and purchased from Merck. The deionized water was Stillman produced with a conductivity of less than 1 μS.

2.7. High Performance Liquid Chromatography (HPLC) for the samples FLT and Ex

UNODC (United Nations Office on Drugs and Crime) method (Recommended methods for the identification and analysis of cannabis and cannabis products 5.4.8 HPLC) was applied. A LiChrospher column (150x4 mm RP-8 with 5 μm particle size), protected with precolumn (4 × 4 mm RP-8 with 5 μm particle size) was used under the following conditions: Column temperature: 30 °C; Mobile phase: acetonitrile and water 80:20 (*V/V*) with an isocratic gradient; Injection volume: 10 μL; Flow rate in the column: 1 mL/min; DAD detector measuring four wavelengths: 220, 240, 210, and 306 nm (maximum absorption at 220 nm); External standards: CBD, THC (Rt of CBD ~ 2.5 min; Rt of THC ~ 3.5 min) for the calibration curve.

2.8. Statistical analysis

The partial least-squares analysis was employed to build calibration models for quantification of THC and CBD in Cannabis extract and flowers, using the spectroscopy skin of Simca14 (Umetrics, Sweden). Spectral pre-processing was performed using the spectral filters add-in. The correlation coefficients of both X and Y matrices (R2X and R2Y), the predictivity coefficient (Q2), root mean square error of estimation (RMSEE), and the root mean square error of cross-validation (RMSEEcv) were used as the main statistical indicators. The VIP and coefficient plots were used for further analysis of the models. The predictive capability of the models was evaluated on separate predictive sets and the root mean square error of prediction (RMSEP) was determined for each model.

3. Results and discussion

3.1. HPLC assay of target cannabinoids in all samples (FL, FLT and Ex)

HPLC analysis confirmed the expected ratio of THCA/CBDA content in the FL samples showing the dominant presence of the THCA over CBDA content in the FL1 medical cannabis and prevailing amount of CBDA over THCA content in FL2 medical cannabis

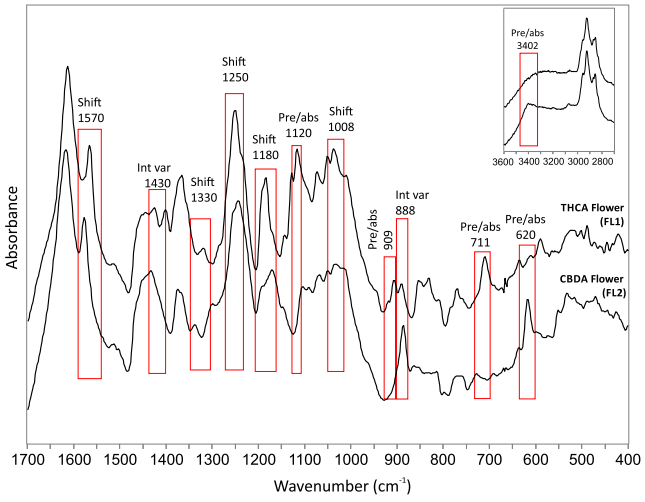

Fig. 2. FTIR spectra of THCA and CBDA dominant flowers. The discussed spectral differences are marked in rectangles.

Table 2
Tentative assignment of the discriminating IR bands found in the spectra of cannabis flowers with strikingly different THCA and CBDA content.

THCA dominant flower (FL1)	CBDA dominant flower (FL2)	Discrimination reason	Tentative assignment
–	3402 s	Absence/presence	ν(OH), OH in para-position to carboxylic group
1565 m	1575 m	Shift	ν(–C=C–), aromatic ring
1427vw	1432 m	Intensity variation	$\delta(CH_2)$ + $\delta(CH_3)$, aliphatic
1320w	1337w	Shift	$\delta(CH_2)$, fibers
1252vs	1244vs	Shift	ν(C–OH), carboxylic group
1186 s	1168 m	Shift	ν(C–OH), OH in ortho-position to the carboxylic group
1120 m	–	Presence/absence	ν_{as}(C–O–C), C_{aryl}–O–$C_{aliphatic}$ group
1008w	1016w	Shift	ν(C–C), aliphatic chain
909w	–	Presence/absence	$\nu_s(C–O–C)_{in\ plane}$, C_{aryl}–O–$C_{aliphatic}$ group
887vw	888 s	Intensity variation	$=CH_2$ wagging, R'R">C=CH_2 group
711 m	–	Presence/absence	$\delta(C–O–C)_{in\ plane}$, C_{aryl}–O–$C_{aliphatic}$ group
–	620 s	Absence/presence	/

Intensity codes: s – strong; m – medium; w – weak; v – very.

Table 3
The bands occurring in the mid-infrared spectra of native and decarboxylated cannabis sativa flowers and extracts, compared to the corresponding available literature data for pure cannabinoids and other similar cannabis matrices providing tentative band assignments. The discriminating bands in the THC and CBD spectra are given in bold. The maxima of the CBDA bands were given for the bands at 883 and 620 cm^{-1} whereas the others (given in italic) were estimated from Ref. [28].

This work THCA flower, FL1	This work CBDA flower, FL2	This work Decarboxyl. Flower, FLT	This work Decarboxyl. extract	This work THCA	This work THC	Ref. [28] CBDA	This work CBD	Ref. [21] Lignin and fibers	Ref. [23] Hemp	Ref. [24] Hemp oil	Tentative IR band assignments [24]	Ref. [25] Hemp and Cannabis (Raman)	Tentative Raman band assignments [25]	Ref. [22] Natural Fibers	Tentative IR band assignments [22]
4000–500	4000–500	4000–500	4000–500	4000–600	4000–600	4000–600	4000–600	2000–600	4000–600	3600–500		1700–700		3600–500	
							3522s								
–	3402s	3600–3100s, br	3600–3100s			*3410s*	**3410vs**		3400s	3474vw	overtone, glyceride ester carbonyl			3600–3000	ν(OH) H-bonded in cellulose and hemicell
2955sh	2955vw	2955w	2955w	2965w	2960sh	*2960sh*	2965w		2950m	3010m	olefinic CH double bond - stretch				
2923s	2923s	2923s	2925s	2924w	2926m	*2930m*	2925s		2920m	2925vs	$\nu_{as}(CH_2)$			2935	ν(CH) cellhemicell
2870vw	2870vw	2870sh	2868sh	2866w	2858m	*2865w*	2871vw								
2853m	2853m	2853m	2856m				2855w			2854vs	$\nu_{sym}(CH_2)$			2862	$\nu(CH_2)$ cellhemicell
2829sh	2829sh	2829sh	2829sh	2828sh	2830sh		2829w								
1733vw	1733vw	1733sh	1703w			*1700w*		1700sh	1720s	1746vs	ester carbonyl (C-O), triglycerides	1691	ν(CO), carboxyl groups	1735	ν(CO) from COOH ester group in hemicell
1614s	1615s	1621s	1621s	1614vs	**1621s**	*1615vs*	1623s	1618-1640vs	1650w	1653vw	CC unsaturated acyl groups	1623	aromatic, THCA	1635	δ(OH) sorbed water
1565m	1575m	1578s	1577s	1563s	**1573s**	*1570s*	1582vs		1594m			1610	ν(C–C) aromatic ringσ(CH), lignin	1595	aromatic ring in lignin
1510vw	1510vw	1510m	1510m	1503vw	**1503m**	*1500vw*	**1510m**	1515s	1510m			1527–1551	CC-(in plane), carotenoids	1502	aromatic ring in lignin
1450sh	1450sh	1460sh	1460sh	1455m, br	1450sh	*1450m*	**1445vs**	1464m	1460m			1455	$\delta(CH_2)$ bending, aliphatic		
1427vw	1432m	1424s	1425s	1401w	**1423vs**	*1430w*	–	1428w	1420m	1200–1400	$\delta(CH_2$ and $CH_3)$ aliphatic groups	1440	$\delta(CH_2) + \delta(CH_3)$ bending, aliphatic	1425	COOH in pectin and COO– vibration
1403vw	–	1375vw	1378vw		1378sh		1375w	1372vw				1376	$\delta(CH_2)$ bending, aliphatic	1375	δ(CH) in cell and hemicell
1365m	1365m	1365vw	1363vw	1366m	1365vw	*1370m*									
1320w	1337w	1347vw	1348vw	1325sh	1343vw		1342vw	1324m	1330m			1321	$\delta(CH_2)$ bending, aliphatic	1315–1335	CH_2 wagging in cell and hemicell
–	1300w	1267w	1267w	1288vw	**1262m**		1278vw	1270w	1270m			1295	THC/THCA	1275	characteristic lignin peak
1252vs	1244vs	1244vw	1244vw	1251vs		*1250vs*	1236vw,sh		1230s			1267	C–O stretching (aromatic), lignin	1240	C–O of acetyl in pectin or hemicell
1234vw	–	1234w	1234w	1233sh	1232w		**1215vs**	1217m				1212–1228	δ(C–C–H), aliphatic and xylan		
1186s	1168m	1183w	1183m	1184vs	**1180s**	*1170m*	1171vw					1185	ν(C–O–H) next to aromatic + σ(CH), xylan		
1145vw	1145vw	–	1156w				1150vw	1152vw	1160w			1155	ν_{as}(C–C) ring breathing, carb + cellulose	1160	δ_{as}(C–O–C)
1120m	–	1129w	1129w	1124sh	1128m		1135vw							895–1125	ν(C–O) and ring modes
		1111vw	1113vw	1118m	1111w	*1107w*						1114	ν_{sym}(C–O–C) and C–OH bending, cellulose	895–1125	ν(C–O) and ring modes
–	1099vw	1091w	1097vw		1090vw	*1097vw*	1098vw		1100m	1093–1120	ν(C-O) ester groups	1084	ν(C–O) + ν(C–C) + δ(C–O–H), carbohydrates	895–1125	ν(C–O) and ring modes
1074vw	1072vw			1075w		*1072w*	1079vw							895–1125	ν(C–O) and ring modes
1050vw	1050vw	1050sh	1050m	1053w		*1050vw*	1051w							895–1125	ν(C–O) and ring modes
1034w	1032w	1038 s	1040 s	1040w	**1038vs**	*1040w*	1032vw	1034w	1030vs					895–1125	ν(C–O) and ring modes

(*continued on next page*)

Table 3 (*continued*)

This work THCA flower, FL1	This work CBDA flower, FL2	This work Decarboxyl. Flower, FLT	This work Decarboxyl. extract	This work THCA	This work THC	Ref. [28] CBDA	This work CBD	Ref. [21] Lignin and fibers	Ref. [23] Hemp	Ref. [24] Hemp oil	Tentative IR band assignments [24]	Ref. [25] Hemp and Cannabis (Raman)	Tentative Raman band assignments [25]	Ref. [22] Natural Fibers	Tentative IR band assignments [22]
1008w	1016w	1009w	1004w	1011vw	996vw	*1007vw*	1019,1001w					993 + 1000	ν_3(C–CH3) + phenylalanine, careotenoids + proteins	895–1125	ν(C–O) and ring modes
		921vw	920vw	907vw	917sh		960w	913vw				916	ν_{sym}(C–O–C) in plane, cellulose + lignin	895–1125	ν(C–O) and ring modes
909w	–	908vw	908w	892vw	906vw		896m							895	beta links in cellulose
887vw	888s	880sh	880sh		877vw	883s	**883m**								
858vw	858vw	847sh	848sh	852m, br		*860w*	851m								
834vw	830vw	835s, br	835w,br	834w	**835m, br**	*818m*	827w		840w			835	THC/THCA		
774vw	773w	770w	784w	772w	770vw	*775w*	802w					780	THC/THCA		
711m	–	726w	728w	713m	722w	*730w*	728w		722m		CH_2 rocking + CH out-of-plane				
–	620 s	–	660w	657vw	680vw	620 s	646w								

Intensity codes: s – strong; m – medium; w – weak; v – very.

(Table 1). The total content of both THCA and THC in the FL1 cannabis plant calculated as total THC was 18.42 wt% and the content of the CBDA and CBD calculated as CBD was below 0.2 wt%. Rather opposite content was observed in the FL2 cannabis flower [20.33 wt% total CBD vs 0.79 wt% total THC] (Table 1).

3.2. IR spectroscopy

3.2.1. FL samples

The description and assignment of the IR spectra was conducted following the available literature with an emphasis of the analytical bands responsible for differentiation of the cannabinoids of our interest: THCA, THC, CBDA, and CBD (Fig. 1). Firstly, given the need for precise spectral examination, two air-dried, non-thermally treated flowers (FL1 and FL2) were screened (Table 1). The strikingly various content of CBDA and THCA in these flowers enabled to ascribe the bands originating from these cannabinoids because it was assumed that the remaining content of the chemical species of the flower is rather similar and comparable (lignin, cellulose, hemicellulose and terpenes). Namely, the attempt was made to select discriminating spectral regions for THCA and CBDA native flowers that, although depict evident similarities, exhibit marked differences (Fig. 2). The apparent spectral disparity was discussed in terms of: (i) shift of the position of the dominant bands, (ii) absence/presence of discriminating bands and (iii) differences in the intensity of the identical band (Table 2).

The applied approach was advantageous because the cannabis flowers contain various molecule species and was perplexing to specify an infrared band solely to a particular cannabinoid or terpene analyte. Thus, the bands in the dominant THCA flower emerge at 1120, 909, and 711 cm^{-1} that are not registered in the CBDA flower where, on contrary, the bands at 3402 and 620 cm^{-1} evolved (Table 2, Fig. 2). An intensity increase of the 888 cm^{-1} band in the CBDA plant was observed, largely diminishing in the spectrum of the THCA flower (Fig. 2). Another apparent difference among both spectra is associated with a marked shift of the medium to strong pair-analogues around 1570, 1250, and 1180 cm^{-1} (Fig. 2, Table 2). However, due to the similar structural formula of the tracked cannabinoids, we found all these regions as reliable indicators to fortify the discrimination of the THCA and CBDA molecular entities, but we will firstly focus on the interpretation towards the absent/present bands and further encompass the assignment in the appointed shifting band regions.

The band at 3402 cm^{-1} found in the CBDA dominant flowers is attributed to the stretching OH vibration from the aromatic OH group situated in para-position to the carboxylic group fragment (Fig. 1c, d). This OH group is not present in the THC and THCA molecules (Fig. 1a, b) and therefore lacks in the spectrum of the FL1 cannabis cultivar (inset in Fig. 2, Table 2). On contrary, the bands at 1120 and 909 cm^{-1} as well as the band at 711 cm^{-1} in the spectrum of THCA flowers (missing in the CBDA flower spectrum) could be related to the aryl-alkyl ether group present in the THCA molecules (CBDA molecule lacks such moieties, Fig. 1) and assigned to antisymmetric and symmetric C–O–C stretching, and ring symmetric C–O–C bending vibration, respectively [20]. On the other hand, the $=CH_2$ wagging vibrations from the (R'R''>C=CH_2 group) gave rise to the strong 888 cm^{-1} band registered in the CBDA flower spectrum because the THCA compound lacks unsaturated C=C linkage in this structural position (Fig. 1, Table 2).

Further focus on the assignment in the appointed shifting band regions infers that the 1570 cm^{-1} maximum is attributed to the stretching ν(–C=C–) vibration within the aromatic rings in the lignin, cellulose and the remaining cannabis species. C–H bending vibrations from the CH_2 and CH_3 aliphatic groups in these compounds are observed around 1430 cm^{-1}, and the ν(C–O–H) vibra-

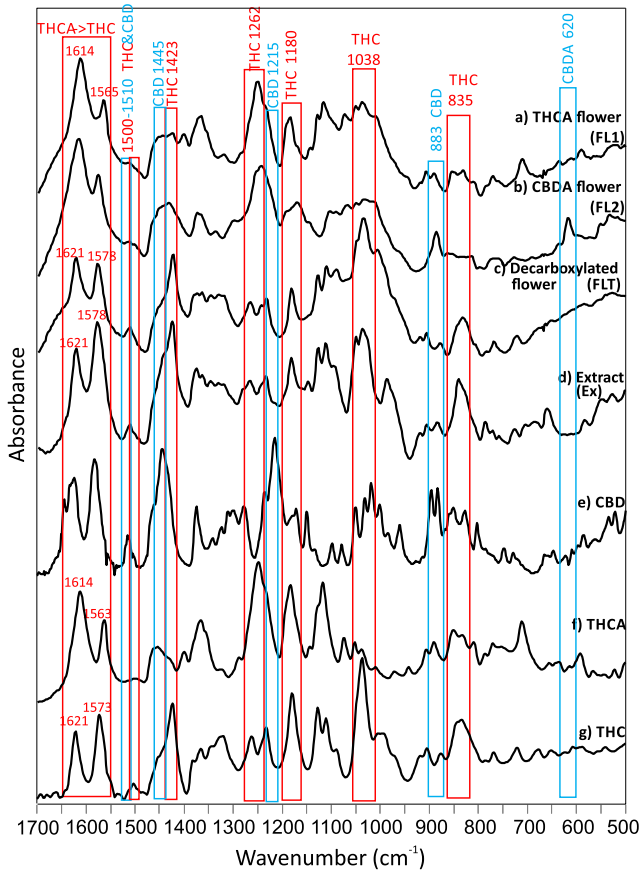

Fig. 3. FTIR spectra of: (a) THCA dominant flower, (b) CBDA dominant flower, (c) decarboxylated flower, (d) cannabis extract sample, (e) CBD, (f) THCA, (g) THC. The discussed spectral regions sensitive to THC and CBD(A) content are marked with red and blue rectangles, respectively.

tion next to the carboxylic group around 1180 cm^{-1}. However, the most intense absorption around 1250 cm^{-1}, slightly shifted among the THCA and CBDA spectra, is ascribed to the ν(C–OH) vibration from the carboxylic group since upon decarboxylation the intensity of this band majorly decreases (see forthcoming discussion). Although the precise assignment of these bands poses a great challenge due to the complex matrix of the samples, the proposed tentative assignment (Table 2, Fig. 2) was made in accordance with the limited IR spectral literature data for hemp and cannabis-related specimens [21–24] and the recent non-destructive Raman studies aimed to differentiate between hemp and cannabis [25,26].

3.2.2. Thermally treated (decarboxylated) Cannabis flowers and extracts

It is worth emphasizing that the decarboxylation protocol was delivered for non-origin correlated THC(A) and CBD(A) matrices of 45 thermally-treated flowers and 34 extracts. The idea was driven to develop a proper protocol that can sufficiently and reliably estimate the content of the major CBD and THC in any randomized series of flower and extract samples. For ease of interpretation, we have also considered the fact that the content of the acidic cannabinoids THCA and CBDA in the non-thermally treated samples is reasonably higher compared to the thermally treated flowers. Namely, flowers dominantly contain the acidic forms of the cannabinoids which upon careful temperature action are decarboxylated and converted to THC and CBD, respectively. The results from the IR spectra filtered the most important regions that reflect (i) the major differences appearing among the different fresh flowers, and (ii) other regions where the major differences occur among the decarboxylated flowers and extract samples in comparison to the spectra of the starting fresh flowers. These spectral outcomes were found complementary to the chemometric results (see further discussion).

To the best of our knowledge, the literature lacks IR band assignments for pure THCA, CBDA, THC and CBD, though the spectral appearance of these compounds in the native form can be found in the German Pharmacopeia [8] (CBD), Specac App Note [27] (CBD), Bruker App note [28] (THC, THCA, CBDA), and PerkinElmer App note [29] (THCA). The IR spectra of the acidic forms of the cannabinoids of interest (THCA, CBDA) were only presented (not discussed) by Hazekamp et al. [30] who isolated these compounds from the concentrated ethanolic solutions (mixed with KBr), subsequently evaporating the ethanol under vacuum. The band positions and intensities were extracted from the spectra of the THCA/THC and CBD powder standards whereas the IR bands from the CBDA cannabinoid were taken from the mentioned reference [28] (Table 3, Fig. 3). These spectra were additionally used and compared with the spectra of the native and decarboxylated flowers and extracts that markedly helped in the band assignments (Table 3, Fig. 3).

The most abrupt spectral difference evidenced upon decarboxylation of the flowers is depicted by the increase of the intensity of the bands around 1510, 1430, 1260, 1180, 1040 and 835 cm^{-1} (Fig. 3a–c, rectangular regions). The obtained result infer that the emerging bands most likely arise from the vibrations within the THC and CBD units whose content increased upon heating, as the presence of the corresponding acidic forms is majorly reduced. The drawn assumptions were confirmed by comparison of the analyzed native and decarboxylated spectra with the spectra of pure cannabinoids (Fig. 3e, f, g). Thus, the medium band at 1510 cm^{-1}

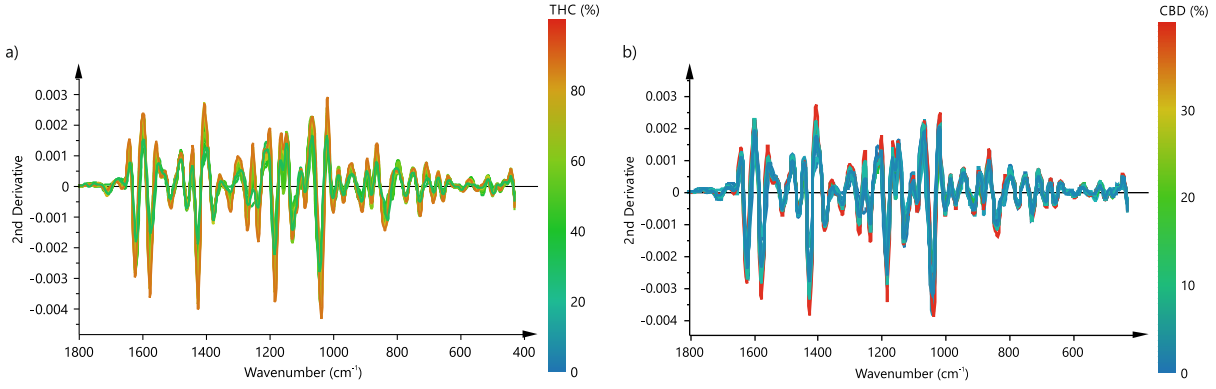

Fig. 4. Overlaid spectra from the calibration and prediction sets used in the statistical model for Cannabis extracts, colored according to THC (a) and CBD (b) content.

occurs from both the CBD and THC (very weak in the spectra of the acidic forms) (Fig. 3) and intensity increase upon flower decarboxylation infers increase of their content. In addition, the striking rise of the band at 1424 cm^{-1} (Fig. 3a, b vs Fig. 3c, d) is attributed to the vibrations from the THC molecules since its intensity dominates in the IR spectrum of the pure THC (Fig. 3g) and the CBD lacks this IR absorption band (Fig. 3e, Table 3). A similar conclusion is derived for the bands at 1267, 1038 and 835 cm^{-1} in the decarboxylated flower spectrum (Fig. 3c) that are the strongest band in the THC and either very weak or absent in the CBD counterpart (Table 3). Furthermore, the bands at 1621 and 1578 cm^{-1} are *blue shifted* in the heated samples (Fig. 3c, d) in comparison to fresh THCA dominant flowers (1614 and 1565 cm^{-1}, Fig. 3a) and pure THCA spectrum (1614 and 1563 cm^{-1}, Fig. 3f). This outcome strongly reflects that, upon heating, the THCA conversion to THC might be successfully monitored by infrared spectroscopy even in the complex matrix. Similarly, the recent Raman spectroscopy work for non-invasive and non-destructive differentiation between

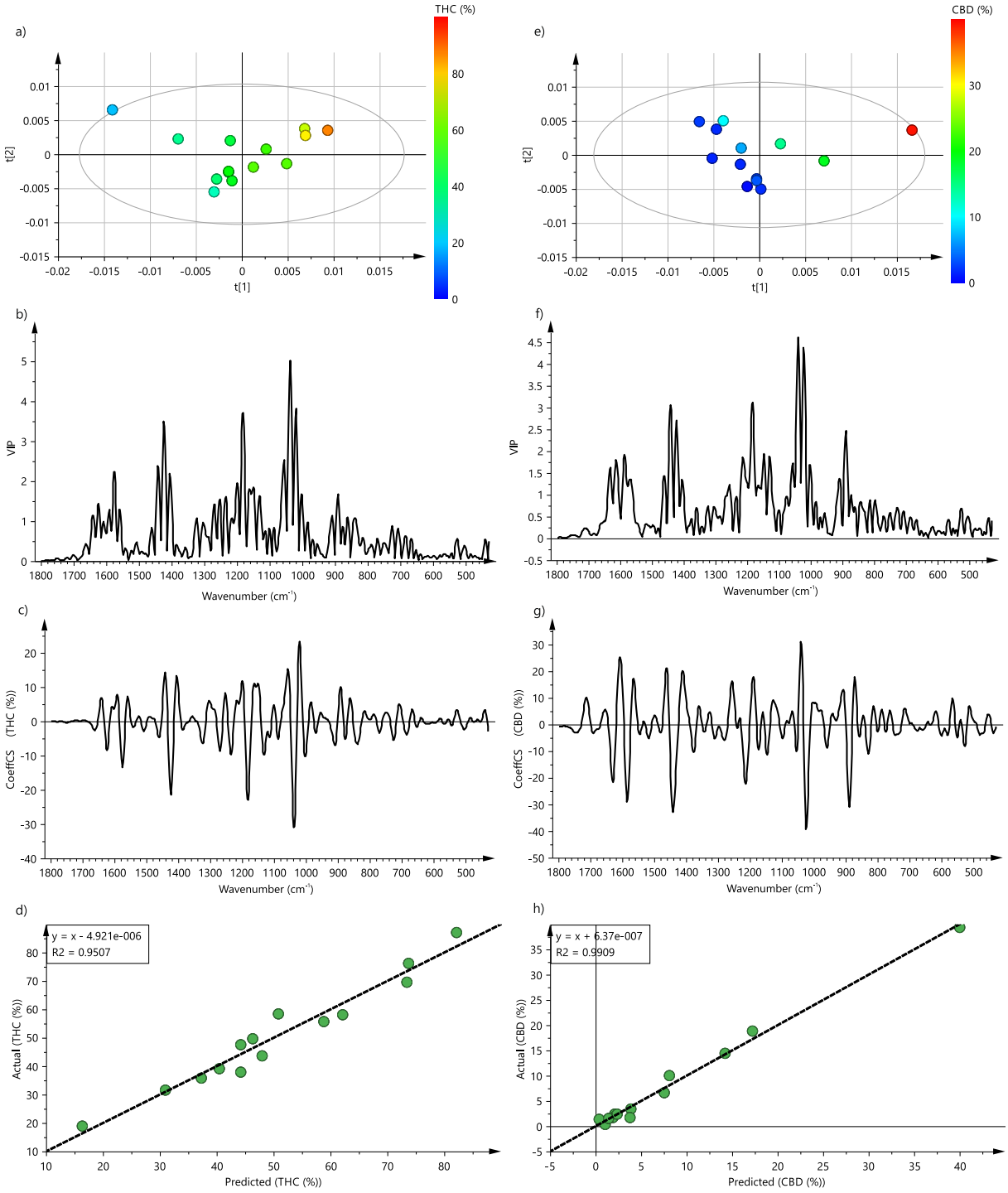

Fig. 5. Main Cannabis extract PLS model statistical output: (a) score scatter plot, (b) VIP plot, (c) coefficients plot, (d) actual vs predicted plot for THC quantification, and (e) score scatter plot, (f) VIP plot, (g) coefficients plot, (h) actual vs predicted plot for CBD quantification.

hemp and cannabis attributed the bands at 1623 and 1295 cm^{-1} to THCA/THC species assigning the former one to their aromatic ring vibration [26].

On contrary, the heated flowers (Fig. 3c) contracted the intensities of strong 888 and 620 cm^{-1} bands found in the fresh CBDA-rich flowers (Fig. 3b) that are obviously attributed to the CBDA molecules. Namely, these bands are crucial to determine the presence of the CBDA compound (spectrum not shown here) appearing as the strongest peaks in the pure sample [28] (Table 3). Moreover, their absence in the THCA counterpart infers that these bands are analytical signatures to follow the transformation of CBDA into CBD. It is also worth mentioning that the IR spectra of the decarboxylated flowers made possible to discriminate between CBDA and CBD on one hand and the THCA and THC on the other. Moreover, the spectra of the decarboxylated flowers and the fabricated extracts are practically identical (Fig. 3c, d). Thus, the band discussion for the spectrum of the decarboxylated flower is also valid for the bands in the spectrum of the cannabis extract. This approach derived from the IR results for the native and decarboxylated flowers was further confirmed by the chemometric model encompassing the most discriminating bands at 1580, 1430, 1183 and 1040 cm^{-1} as predictors for THC concentration (see forthcoming discussion).

3.3. Chemometric approach for MIR spectra quantification of THC and CBD

PLS approach was employed for building separate calibration models for the quantitative determination of CBD and THC from flowers and extract samples. The HPLC determined concentrations of CBD and THC were appointed as dependent (Y) variables, while the MIR spectra were denominated as independent (X) or predictor variables.

3.3.1. Statistical models for decarboxylated Cannabis extracts

Fourteen MIR spectra acquired from different cannabis extract samples were used to construct the calibration set whereas the remaining 20 spectra were used for the prediction set. The CBD and THC concentrations in the samples varied between 0.38–39.2% and 18.93–86.99%, respectively (HPLC determined). Only the spectral region of 1800–400 cm^{-1} was used for the statistical modeling because the ATR diamond crystal exhibit two-photon broad IR absorbance bands between 2600 and 1900 cm^{-1} that reduce the signal-to-noise ratio (SNR), and the MIR region above 2600 cm^{-1} did not contain any specific bands originating from the molecules of interest. The preliminary analysis of the models revealed that Savitskzy-Golay smoothing and the second derivative of the native MIR spectra resulted in best-fit parameters for R2Y, R2X (the cumulative explained fraction of the variation in the Y and X blocks of variables) and Q2 (the cumulative fraction of total variation in the dependent variables, that can be predicted with the model). The overlaid spectra from the calibration and prediction set, colored according to the THC and CBD content of the samples are presented in Fig. 4a and b. Considering that CBD and THC were not the sole components in the extract and that the samples originated from different sources (different Cannabis flowers, extraction methods etc.), it is logical to assume that some transformation of the spectra will be needed to separate and potentiate the specific bands with quantitative relationship to the components of interest. Therefore, in the further part, only the model based on the abovementioned transformation will be presented and discussed.

Three main components were extracted from the PLS model for quantification of THC with 0.934, 0.951 and 0.909 for R2X, R2Y and Q2. The score scatter plot (Fig. 5a) for this model reveals distinctive pattern of the sample variances that can be traced to the concentration of THC in the samples. Indeed, these plots reveal how

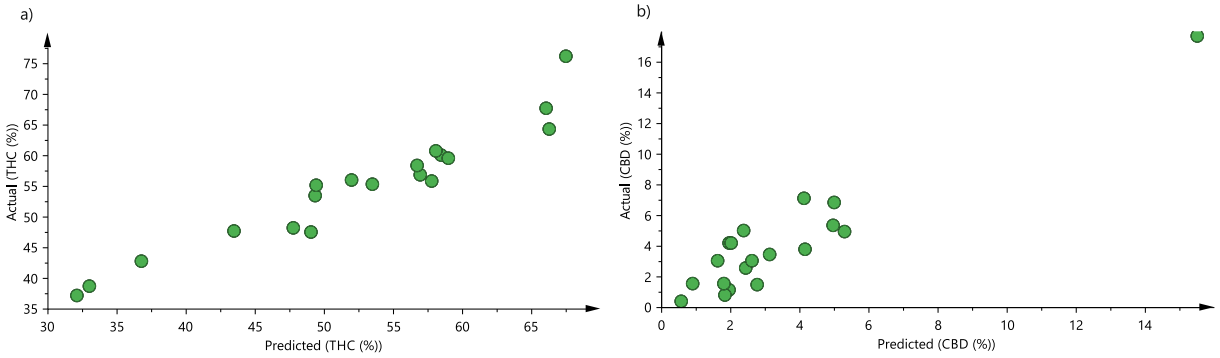

Fig. 6. Actual versus predicted plot for the prediction set of the Cannabis extract PLS models for calculation of THC (a) and CBD (b) content.

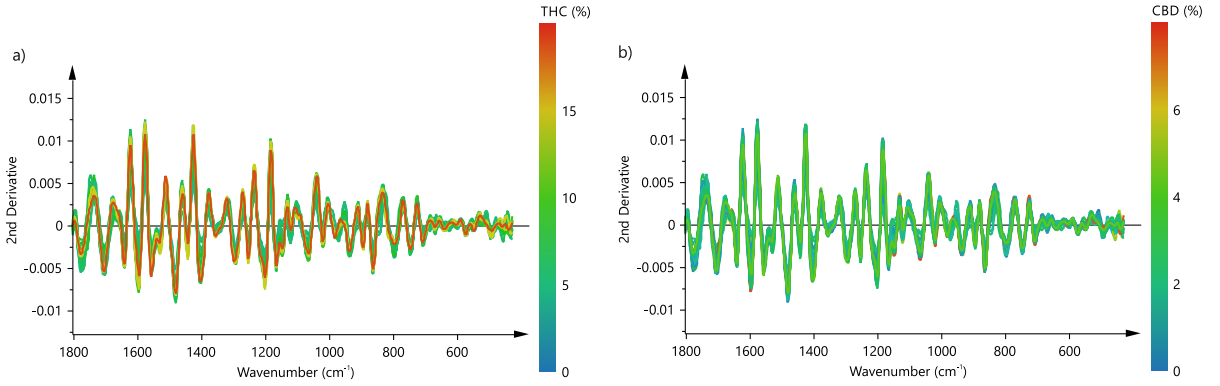

Fig. 7. Overlaid spectra from the calibration and prediction sets used in the statistical model for Cannabis flowers, colored according to THC (a) and CBD (b) content.

the X variables are related to each other [31]. In this model, there is a clear trend of distinction among the spectra (X variables) along the t1 vector (the first component) related to the THC concentration of the samples, thus pointing out the dominant role of the first component in the overall prediction capability of the model. Furthermore, the VIP (Variance important for projection) plot (Fig. 5b) reveals the spectral regions with the utmost importance in the regression model. The bands with VIP factor larger than 1, are usually considered as important both for explaining the variations in the X matrix as well as to correlate with the Y variables [32]. The spectral regions around 1040, 1425, 1183 and 1577 cm^{-1} demonstrate the largest VIP factors in the model and should be considered as main predictors for the THC concentration. The latter could be additionally confirmed with the coefficient plot (Fig. 5c), where the mentioned spectral regions are assigned with the largest regression coefficients. The plotted results of actual (HPLC determined) versus the predicted THC concentrations (MIR spectra) are presented in Fig. 5d, and the RMSEE (Root Mean Square Error of Estimation) of 4.67% indicates the fit of the observations to the model. The RMSEcv for this model is 5.25% and it is an analogous measure to RMSEE, but estimated using a cross-validation procedure. The RMSEE and RMSEcv are descriptors

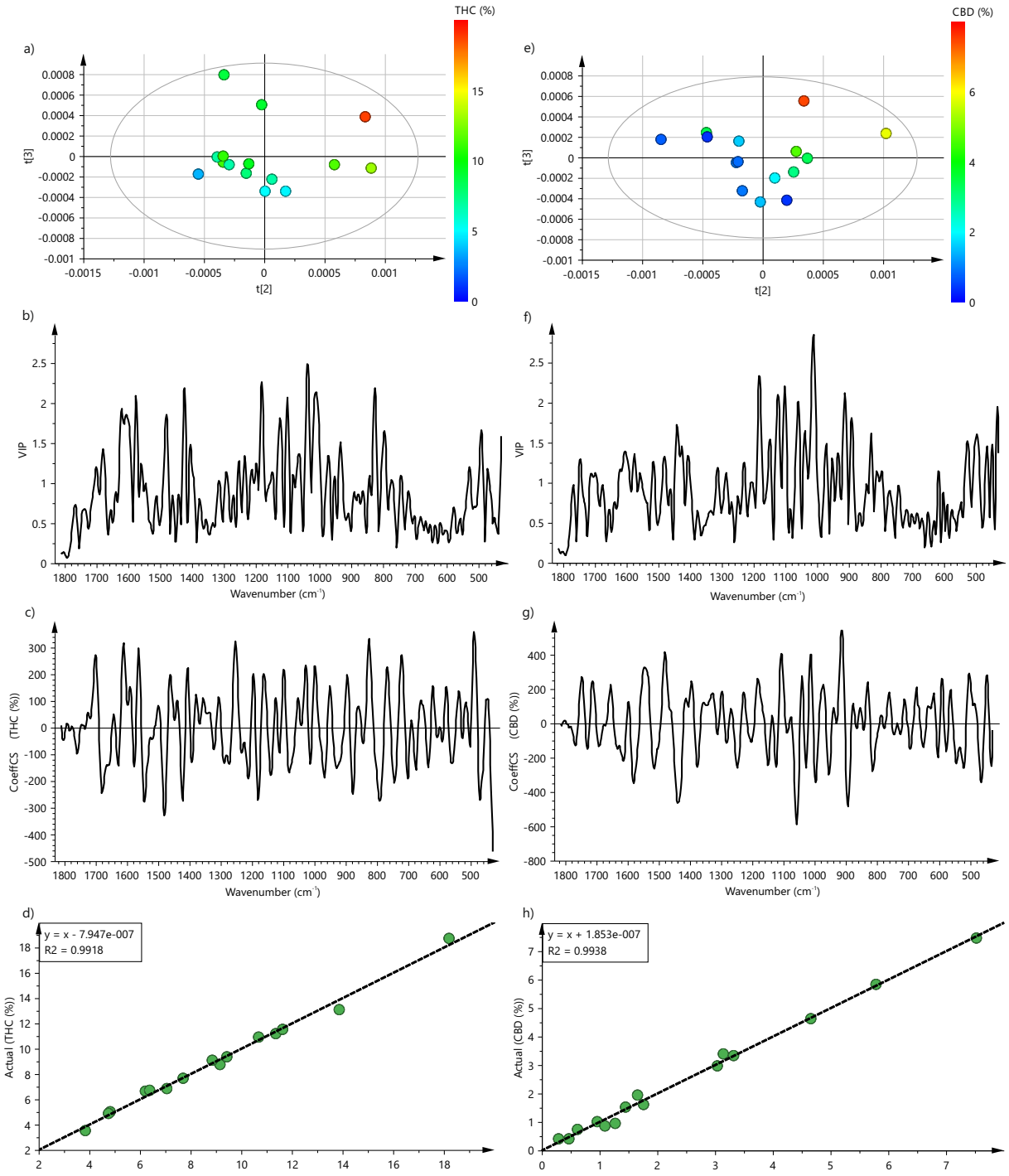

Fig. 8. Main Cannabis flower PLS model statistical output (a) score scatter plot, (b) VIP plot, (c) coefficients plot, (d) actual vs predicted plot for THC quantification and (e) score scatter plot, (f) VIP plot, (g) coefficients plot, (h) actual vs predicted plot for CBD quantification.

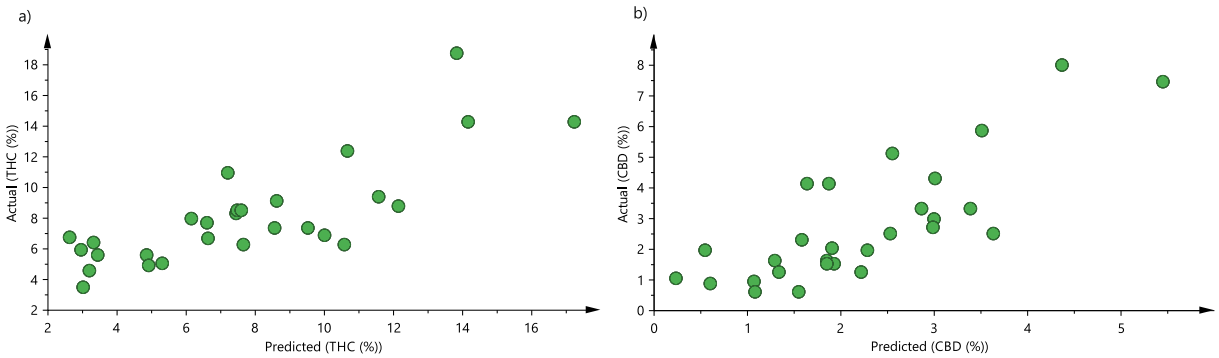

Fig. 9. Actual versus predicted plot for the prediction set of the Cannabis flower PLS models for calculation of THC (a) and CBD (b) content.

for the absolute accuracy of the model, and the values reported here should be expected, taking into consideration the variable origin of the samples (different matrices), number of samples, the employed concentration range, and the real limits of the analytical technique (ATR-MIR).

Three main components were also extracted from the CBD quantification PLS model with 0.936, 0.991 and 0.972 for R2X, R2Y and Q2. In this model, the score scatter plot (Fig. 5e) also presents a distinctive pattern related to the CBD concentration in the samples that follow a diagonal line between both score vectors (t1/t2), indicating that both the first and second component has significant capabilities for prediction of the Y variable. The VIP plot (Fig. 5f) demonstrated that the same spectral regions of the previous model (1577, 1425, 1183, and 1040 cm^{-1}), with an addition of the region around 880 cm^{-1} (also determined by the IR spectra, Fig. 3). These regions bear the largest VIP factors, and at the same time, the mentioned spectral ranges are assigned with the largest regression coefficients (Fig. 5g). The plot of actual versus predicted CBD concentrations (Fig. 5h) reveals a better fit of the points relative to the previous THC model with 1.21 and 2.62% for RMSEE and RMSEcv.

The predictive capabilities of both models were evaluated separately on a prediction (training) set of 20 extract samples of various origin and the results are presented in Fig. 6a and b. The root mean square error of prediction, (RMSEP) for THC and CBD PLS quantification models were 3.79 and 1.44%, respectively, thus confirming the previous accuracy descriptors and ruling out the possible bias of the calibration models.

3.3.2. Statistical models for decarboxylated Cannabis flowers

The PLS models for the quantification of THC and CBD in decarboxylated Cannabis flowers also employed the second derivatives of the raw MIR spectra (1800–400 cm^{-1}) with Savitsky-Golay smoothing. The overlaid spectra from the 45 samples used in the calibration and prediction set, colored according to the THC and CBD content of the samples are presented in Fig. 7a and b. As in the previous case, such transformation was chosen as the most optimal regarding the main fit parameters (R2Y, R2X and Q2) in comparison to the raw, SNV and first order derivative MIR spectra models. Such data transformation is often considered as a necessity in cases where spectra from complex matrices are obtained and the main quantification related bands are overlapped with other components present in the sample.

The THC PLS quantification model was build using transformed spectra acquired from 15 decarboxylated samples with various THC content and origin (30 samples were left for the training set). Five main components were extracted from the model explaining 97.2% of the variations in the X-variables, and producing a high correlation coefficient R2Y = 0.992 with appropriate predictability (Q2 = 0.891). The score scatter plot of the second and third component vectors reveal the THC content related pattern, where the THC content increases as a function of the score in both components (Fig. 8a). The model VIP plot (Fig. 8b) exposes the bands that are related to the THC content in the flowers. The spectral regions around 1620, 1610, 1578, 1425, 1180, 1038, 1010 and 825 cm^{-1} which are similar to the ones reported in the extract PLS models, are also assigned with large VIP factors. The coefficient plot confirms the previous findings, where the abovementioned spectral regions with the highest VIP factors, are also assigned with the highest regression coefficients (Fig. 8c). The RMSEE and RMSEEcv derived from the actual versus predicted THC concentrations plot (Fig. 8d) were 0.43 and 1.53%. The complexity of the sample (plant tissue), the variability of the samples in regards to their origin and horticultural maturity, as well as the non-uniformity of the plant material and the flower-ATR crystal contact should be considered as main factors that govern the accuracy descriptors.

Five main components were extracted for the PLS modeling for CBD content quantification of the Cannabis flowers with R2X = 0.969, R2Y = 0.994 and Q2 = 0.66. As in the previously described model, the score scatter plot of the second and third main components vector presents a distinctive pattern associated with the CBD content in the samples (Fig. 8e). The bands around 1440, 1185, 1100, 1010, 911, 888, and 826 cm^{-1} demonstrated the largest VIP factors in the MIR spectra (Fig. 8f). The mentioned bands were assigned with the highest regression coefficients (model coefficient plot Fig. 8g), thus confirming their association with the CBD content. The actual versus predicted plot (Fig. 8h) of the samples demonstrates a satisfactory level of correlation and the accuracy model parameters RMSEE and RMSEEcv were 0.21 and 1.41%.

To evaluate the predictive capability of the abovementioned PLS models for quantification of THC and CBD in decarboxylated Cannabis flowers, a separate prediction (training) set of 30 samples of different origin was employed. The correlation plots of actual versus predicted THC and CBD content are presented in Fig. 9a and b, and the models RMSEP was 2.32% and 1.33% for quantification of THC and CBD, respectively. The RMSEP values are in good agreement with the accuracy descriptors of the models and confirm the presented predicting capability of the models in a separate independent set of samples.

4. Conclusion

In the present work, we have described a stepwise approach in the utilization of ATR-MIR spectroscopy for quantification of the main critical parameters in Cannabis flower and extract samples. A detailed assignment of the bands related to the molecules of interest (THC, CBD) was performed in accordance with the avail-

able literature data. Also, the spectral features of the decarboxylation of native flowers were identified, and the acid forms (THCA, CBDA) specific bands were assigned and thoroughly explained. Further, multivariate models were constructed for prediction of both THC and CBD content in extract and flower samples from various origin, and their prediction ability was tested on a separate sample set. The PLS models presented satisfactory R2Y and RMSEP of 0.95 and 3.79% for THC, 0.99 and 1.44% for CBD in the Cannabis extract samples, respectively. Similar statistical indicators were noted for the PLS models for THC and CBD prediction of decarboxylated Cannabis flowers (R2Y and RMSEP were 0.99 and 2.32% for THC, 0.99 and 1.33% for CBD respectively). The VIP plots of all models demonstrated that the THC and CBD distinctive band regions bared the highest importance for predicting the content of the molecules of interest in the respected PLS models. The complexity of the sample (plant tissue or plant extract), the limited number of samples and concentration range, the variability of the samples regarding their origin and horticultural maturity, as well as the non-uniformity of the plant material and the flower-ATR crystal contact (in the case of Cannabis flowers) should be considered as main factors that govern the accuracy descriptors. Nevertheless, it was outlined that the ATR-MIR should be considered as a promising PAT tool for THC and CBD content estimation, in terms of critical material and quality parameters for Cannabis flowers and extracts.

CRediT authorship contribution statement

Nikola Geskovski: Conceptualization, Methodology, Investigation, Formal analysis, Writing - Original Draft. **Gjose Stefkov:** Conceptualization, Methodology, Resources, Writing - review & editing. **Olga Gigopulu:** Investigation. **Stefan Stefov:** Investigation. **Christian W. Huck:** Writing - review & editing. **Petre Makreski:** Conceptualization, Methodology, Investigation, Formal analysis, Writing - Original Draft.

Declaration of Competing Interest

The authors declare that they have no known competing financial interests or personal relationships that could have appeared to influence the work reported in this paper.

References

[1] D. Friedman, J.I. Sirven, Historical perspective on the medical use of cannabis for epilepsy: ancient times to the 1980s, Epilepsy Behav. 70 (2017) 298–301, https://doi.org/10.1016/j.yebeh.2016.11.033.

[2] J. Cherney, E. Small, Industrial hemp in North America: production, politics and potential, Agronomy 6 (2016) 58, https://doi.org/10.3390/agronomy6040058.

[3] S. Zou, U. Kumar, Cannabinoid receptors and the endocannabinoid system: signaling and function in the central nervous system, Int. J. Mol. Sci. 19 (2018) 833–856, https://doi.org/10.3390/ijms19030833.

[4] R.L. Pacula, D. Powell, P. Heaton, E.L. Sevigny, Assessing the effects of medical marijuana laws on marijuana use: the devil is in the details, J. Policy Anal. Manage. 34 (2015) 7–31 (accessed August 29, 2019).

[5] R. Brenneisen, Chemistry and Analysis of Phytocannabinoids and Other Cannabis Constituents, in: Marijuana and the Cannabinoids, Humana Press, Totowa, NJ, 2007: pp. 17–49. https://doi.org/10.1007/978-1-59259-947-9_2.

[6] E.B. Russo, Cannabidiol claims and misconceptions, Trends Pharmacol. Sci. 38 (2017) 198–201, https://doi.org/10.1016/j.tips.2016.12.004.

[7] L.M. Borgelt, K.L. Franson, A.M. Nussbaum, G.S. Wang, The pharmacologic and clinical effects of medical cannabis, Pharmacother. J. Hum. Pharmacol. Drug Ther. 33 (2013) 195–209, https://doi.org/10.1002/phar.1187.

[8] Die, Allgemeinen Vorschriften" zu Ph. Eur., DAB und DAC/NRF gelten für alle Monographien und sonstigen Texte. DAC/NRF 2016/2, C-052, 2016.

[9] Pharmacopoea Helvetica 11.3, Swissmedic, Bern, 2019.

[10] European Pharmacopoeia (Ph. Eur.) 10th ed., EDQM – European Directorate for the Quality of Medicines, Strasbourg, 2019.

[11] R. Upton (Ed.), American Herbal Pharmacopoeia, American Herbal Pharmacopoeia, Santa Cruz, CA, 2019.

[12] E. Borroto Fernandez, V. Peterseil, G. Hackl, S. Menges, E. Meijer, C. Staginnus, Distribution of chemical phenotypes (Chemotypes) in European agricultural hemp (*Cannabis sativa* L.) cultivars, J. Forensic Sci. 65 (2020) 715–721, https://doi.org/10.1111/1556-4029.14242.

[13] C. Burnier, P. Esseiva, C. Roussel, Quantification of THC in Cannabis plants by fast-HPLC-DAD: a promising method for routine analyses, Talanta 192 (2019) 135–141, https://doi.org/10.1016/J.TALANTA.2018.09.012.

[14] J. Woodcock, The concept of pharmaceutical quality, Am. Pharm. Rev. 7 (2004) 10–15 (accessed August 29, 2019).

[15] L.X. Yu, G. Amidon, M.A. Khan, S.W. Hoag, J. Polli, G.K. Raju, J. Woodcock, Understanding pharmaceutical quality by design, AAPS J. 16 (2014) 771–783, https://doi.org/10.1208/s12248-014-9598-3.

[16] FDA, Guidance for Industry PAT - A Framework for Innovative Pharmaceutical Development, manufacturing, and Quality Assurance, 2004. http://www.fda.gov/cvm/guidance/published.html (accessed March 9, 2019).

[17] C. Sánchez-Carnerero Callado, N. Núñez-Sánchez, S. Casano, C. Ferreiro-Vera, The potential of near infrared spectroscopy to estimate the content of cannabinoids in *Cannabis sativa* L.: a comparative study, Talanta 190 (2018) 147–157, https://doi.org/10.1016/J.TALANTA.2018.07.085.

[18] J. Espel Grekopoulos, Construction and validation of quantification methods for determining the Cannabidiol content in liquid pharma-grade formulations by means of near-infrared spectroscopy and partial least squares regression, Med. Cannabis Cannabinoids 2 (2019) 43–55, https://doi.org/10.1159/000500266.

[19] B.T. Borille, M.C.A. Marcelo, R.S. Ortiz, K. de C. Mariotti, M.F. Ferrão, R.P. Limberger, Near infrared spectroscopy combined with chemometrics for growth stage classification of cannabis cultivated in a greenhouse from seized seeds, Spectrochim. Acta Part A Mol. Biomol. Spectrosc. 173 (2017) 318–323, https://doi.org/10.1016/J.SAA.2016.09.040.

[20] A.P. Kilimov, M.A. Svechnikova, V.I. Shevchenko, V.V. Smirnov, F.V. Kvasnyuk-Mudryi, S.B. Zotov, Infrared spectra of cyclic ethers and their derivatives - I. Pecularities in the skeletal vibrations of the tetrahydrofuran ring, Chem. Heterocycl. Compd. 3 (1969) 467–471, https://doi.org/10.1007/BF00481572.

[21] J.C. del Río, A. Gutiérrez, I.M. Rodríguez, D. Ibarra, Á.T. Martínez, Composition of non-woody plant lignins and cinnamic acids by Py-GC/MS, Py/TMAH and FT-IR, J. Anal. Appl. Pyrol. 79 (2007) 39–46, https://doi.org/10.1016/j.jaap.2006.09.003.

[22] A. Célino, O. Gonçalves, F. Jacquemin, S. Fréour, Qualitative and quantitative assessment of water sorption in natural fibres using ATR-FTIR spectroscopy, Carbohydr. Polym. 101 (2014) 163–170, https://doi.org/10.1016/j.carbpol.2013.09.023.

[23] J. Dorado, G. Almendros, J.A. Field, R. Sierra-Alvarez, Infrared spectroscopy analysis of hemp (Cannabis sativa) after selective delignification by Bjerkandera sp. at different nitrogen levels, Enzyme Microb. Technol. 28 (2001) 550–559, https://doi.org/10.1016/S0141-0229(00)00363-X.

[24] P. Siudem, I. Wawer, K. Paradowska, Rapid evaluation of edible hemp oil quality using NMR and FT-IR spectroscopy, J. Mol. Struct. 1177 (2019) 204–208, https://doi.org/10.1016/j.molstruc.2018.09.057.

[25] L. Sanchez, D. Baltensperger, D. Kurouski, Raman-based differentiation of hemp, cannabidiol-rich hemp, and cannabis, Anal. Chem. 92 (2020) 7733–7737, https://doi.org/10.1021/acs.analchem.0c00828.

[26] L. Sanchez, C. Filter, D. Baltensperger, D. Kurouski, Confirmatory non-invasive and non-destructive differentiation between hemp and cannabis using a hand-held Raman spectrometer, RSC Adv. 10 (2020) 3212–3216, https://doi.org/10.1039/c9ra08225e.

[27] Analyzing the highs and lows of cannabis derivatives with FTIR, 2019. https://www.specac.com/en/documents/application-notes/(web)-an18-05-(analysis-of-legal-cannabis) (accessed October 15, 2020).

[28] H.J.X. Schorno, H.C. Koch, Differentiation of THC and CBD cannabis using FTIR, 2018. https://www.bruker.com/fileadmin/user_upload/8-PDF-Docs/OpticalSpectrospcopy/FT-IR/ALPHA/AN/AN_M157_Differenzierung_Cannabis_FTIR_EN.pdf (accessed October 15, 2020).

[29] B.C. Smith, M.A. Lewis, J. Mendez, Optimization of Cannabis Grows Using Fourier Transform Mid-Infrared Spectroscopy, 2016. https://cdn.technologynetworks.com/tn/Resources/pdf/optimization-of-cannabis-grows-using-fourier-transform-mid-infrared-spectroscopy.pdf (accessed October 15, 2020).

[30] A. Hazekamp, A. Peltenburg, R. Verpoorte, C. Giroud, Chromatographic and spectroscopic data of cannabinoids from Cannabis sativa L., J. Liq. Chromatogr. Relat. Technol. 28 (2005) 2361–2382, https://doi.org/10.1080/10826070500187558.

[31] M. Stojanovska Pecova, N. Geskovski, G. Petrushevski, M. Chachorovska, L. Krsteska, S. Ugarkovic, P. Makreski, Solid-state interaction of ibuprofen with magnesium stearate and product characterization thereof, Drug Dev. Ind. Pharm. 46 (2020) 1–10, https://doi.org/10.1080/03639045.2020.1788067.

[32] L. Makraduli, P. Makreski, K. Goracinova, S. Stefov, M. Anevska, N. Geskovski, A comparative approach to screen the capability of Raman and infrared (Mid- and Near-) spectroscopy for quantification of low active pharmaceutical ingredient content solid dosage forms: the case of alprazolam, Appl. Spectrosc. 74 (2020) 661–673, https://doi.org/10.1177/0003702820905367.